# Ultrafast population transfer to excited valence levels of a molecule driven by x-ray pulses

D. J. Haxton and C. W. McCurdy

Phys. Rev. A **90**, 053426 — Published 21 November 2014

DOI: 10.1103/PhysRevA.90.053426

# Ultrafast population transfer to excited valence levels of a molecule driven by X-ray pulses

D. J. Haxton[1] and C. W. McCurdy[2,3]

[1] *Chemical Sciences, Lawrence Berkeley National Laboratory, Berkeley CA 94720*
[2] *Chemical Sciences and Ultrafast X-ray Science Laboratory, Lawrence Berkeley National Laboratory, Berkeley CA 94720*
[3] *Department of Chemistry, Davis CA 95616*

First-principles quantum mechanical calculations of an intense-field ultrafast two-color core hole stimulated Raman process in nitric oxide are presented. They employ the Multiconfiguration Time-Dependent Hartree-Fock (MCTDHF) method with all 15 electrons active. These calculations demonstrate a robust excitation localized on an atom through a core-electron stimulated Raman transition, the first step in proposed stimulated X-ray Raman spectroscopy experiments. A total population transfer of approximately 41% into valence excited states and 30% ionization is obtained via two concurrent 1.31fs pulses of maximum intensity 0.5 and 3 $\times 10^{17}$ W cm$^{-2}$. It is found that both resonant and nonresonant (via the continuum) Raman transitions contribute. All aspects of these calculations except for AC stark shifts are converged with a modest basis of 11 orbitals, demonstrating the efficiency of MCTDHF for the treatment of nonperturbative electronic dynamics in molecules.

PACS numbers: 31.15.-p, 33.80.Eh, 31.15.xv

## I. INTRODUCTION

Recent proposals for using nonlinear X-ray spectroscopy to study electronic dynamics in molecules involve the creation of coherent linear combinations of valence states using autoionizing, core excited states as intermediates [1–3]. This mechanism permits site specificity; the initial valence excitation is localized on the atomic center supporting the core excitation, and its subsequent evolution across the molecule may be probed by core transitions on other centers. The scientific motivations for the proposed construction of new free-electron laser facilities [4–6] generally include this class of experiments as a principal goal.

One experimental possibility that has received considerable attention is that proposed by Biggs et al. [2], stimulated X-ray Raman spectroscopy with broad band pulses. The simplest version of this idea, called 1D-SXRS, begins with an X-ray pulse having a duration of the order of 100 attoseconds. When tuned below the K-edge of a given atomic center, this broadband pulse stimulates a Raman transition at that center, creating a localized coherent wave packet of valence excited states. A second X-ray Raman pulse probes the fate of the initial valence excitation, again in a site-specific way. Higher dimensional versions of this idea, in particular 2D-SXRS with three broadband X-ray pulses, have also been explored [2]. These ideas have a distinct advantage over proposals for nonlinear spectroscopy, like the extension of optical four-wave mixing to the X-ray regime [7] or the original suggestion for coherent X-ray Raman spectroscopy [8], in that they do not involve phase matching between different X-ray pulses.

However, the proposed SRSX experiment does require that the Raman pump pulse be able to excite a significant amount of population in a coherent valence wave packet so that its evolution can be probed or modified by subsequent Raman scattering events. The motivation of the present study is to investigate conditions that might allow a robust X-ray Raman pump of coherent valence wave packets by intense ultrashort pulses.

We use the MCTDHF method to calculate an ultrafast X-ray stimulated Raman process in nitric oxide. The MCTDHF method includes all nonrelativistic effects, accounting for the presence of all photoionization, autoionization and other loss mechanisms, including strong field effects, e.g., AC Stark shifts, without *a priori* knowledge of the relevant states, with all electrons active. Because these calculations have made no assumptions beyond the nonrelativistic approximation, they clearly demonstrate that short, intense X-ray pulses may drive robust femtosecond population transfer among valence states to create coherent electronic wave packets. Notable experimental and theoretical studies have appeared previously that suggest this conclusion is correct [9–11], but they do not directly address the question we explore here, namely the quantification in an *ab initio* study of the possibility of strong, coherent valence excitation by pulses of femtosecond or shorter duration of the intensities that can be produced by free-electron lasers.

The outline of this paper is as follows. Sec. II explains the Raman processes in the NO molecule studied here. Sec. III describes the MCTDHF method and its implementation including ionization, and gives details of the numerical calculations. In Sec. IV the issue of defining transition energies in MCTDHF calculations, which is not straightforward, is addressed. In Sec. V the Raman signal is reported, and in Sec. VI the population transfer to a coherent valence wave packet is analyzed. We conclude with some final observations in Sec. VII.

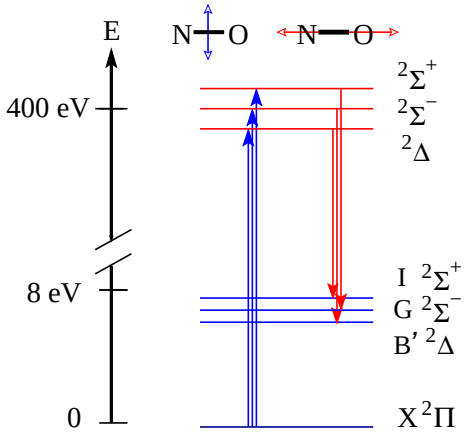


FIG. 1: (Color online) Schematic of the stimulated Raman transitions coherently populating the B′ $^2\Delta$, G $^2\Sigma^-$, and I $^2\Sigma^+$ states of NO.

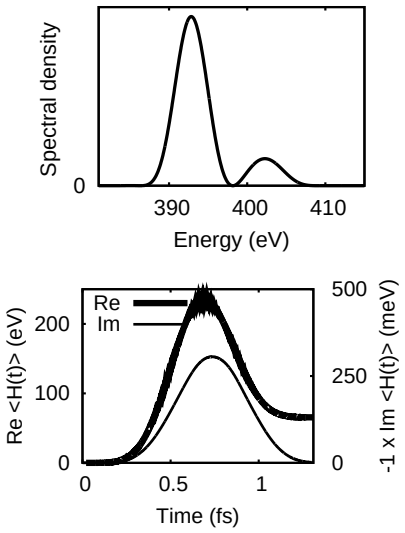


FIG. 2: Top, Fourier transform of the two-color pulse used for the stimulated Raman process; bottom, real and imaginary components of the expectation value of the instantaneous time-dependent Hamiltonian $H = H_0 + \vec{A}(t)\cdot\overrightarrow{\bigtriangledown}$, calculated in the velocity gauge, with 10 orbitals.

## II. STIMULATED RESONANT RAMAN TRANSITIONS NEAR THE NITROGEN K-EDGE

Our goal is to investigate an example of a Raman process that will create a localized excitation that might be probed by a second Raman process. We use a two-color Raman pump pulse consisting of concurrent X-ray pulses with different central energies and and also different polarizations in order to investigate a near optimal case. The transitions may however be driven by pulses with parallel polarization in a gas of unoriented molecules. The pulse duration is chosen to be 1.31 fs, somewhat longer than those in the original SXRS proposal[2]. We have not made a systematic study of the pulse parameters. These studies are intended to establish the tools for optimization of conditions for early experiments to demonstrate SXRS as free-electron lasers and other sources become capable of performing them.

A schematic of the stimulated Raman process we study here is shown in Fig. 1. The NO molecule has a ground state of $^2\Pi$ symmetry having a dominant electronic configuration $1...5\sigma^2 1\pi^4 2\pi^1$. The pump component of the two-color pulse is approximately resonant with core excited electronic states described by a single excitation from the Nitrogen $1s$ orbital into the $2\pi$ shell. The two electrons in the $2\pi$ shell may be coupled in the same manner as they are in the electronic states of $O_2$: $^1\Sigma^+$, $^1\Delta$, and $^3\Sigma^-$, resulting in $^2\Sigma^-$, $^2\Delta$, and $^2\Sigma^+$ electronic states of nitric oxide when coupled to the lone core electron as a doublet. These core hole states are nearly isoenergetic; a single structured peak in the photoionization cross section centered at 400eV photon energy is observed in the experiments of Refs. [12–15]. It has a full width at half maximum of approximately one electron volt, displaying structure attributed to vibrational progressions of these three core excited states [13–15]. These core excited states of NO have been calculated previously [16, 17].

The valence final states are populated through a subsequent transition of a $5\sigma$ electron to N $1s$, giving the configuration $1...4\sigma^2 5\sigma^1 1\pi^4 2\pi^2$, and are labeled as the B′ $^2\Delta$, G $^2\Sigma^-$, and I $^2\Sigma^+$. Potential energy curves for these electronic states have been determined from experiment [18], and UV and electron-impact excitation of valence states of NO has been studied extensively [19–23].

We investigate the configuration in which the molecule is oriented and the polarization vectors are perpendicular. The pump pulse is perpendicular to the bond axis and has maximum intensity $5\times10^{16}$ W cm$^{-2}$; that of the Stokes, in the parallel direction, is $3\times10^{17}$ W cm$^{-2}$. Both pulses have a sine-squared envelope and a duration of 1.31s. For all calculations, the central energies of the two pulses are 402.6 and 393.3eV. Due to errors in the computed transition energies, these are not the energies for the corresponding actual experiment. The calculation corresponds to an experiment performed with pulses about 395.9 and 387.1eV, both substantially red detuned, as discussed in Sec. IV. The Fourier transform of the pulse and the expectation value of the instantaneous Hamiltonian in the velocity gauge are plotted in Fig. 2. As can be seen in Fig. 2, approximately 50eV energy is transferred to the molecule by the two-color stimulated Raman pulse.

## III. METHOD

The multiconfiguration time-dependent Hartree-Fock (MCTDHF) algorithm [24–32] is an adaptive method for calculating nonpertubative electronic dynamics in

molecules. In a recently described numerical implementation [33, 34] that we use here, all electrons are active, all orbitals are time-dependent, and any number of them may be ionized. Because the orbitals are time-dependent, a converged calculation may be obtained using a far smaller orbital basis than would be required in standard configuration interaction treatments. The method accurately represents the competition among various channels involving multiple photon absorption, single and multiple ionization, and excitation into numerous final states that may or may not have been previously identified.

The MCTDHF ansatz describes the wave function of $N$ electrons as a time-dependent linear combination of Slater determinants comprised of time-dependent orbitals,

$$\begin{aligned} |\Psi(t)\rangle &= \sum_{\vec{n}} A_{\vec{n}}(t)|\vec{n}(t)\rangle \\ |\vec{n}(t)\rangle &= \mathscr{A}\left(|\phi_{n_1}(t)\rangle \times ...|\phi_{n_N}(t)\rangle\right) , \end{aligned} \tag{1}$$

where $\mathscr{A}$ is the antisymmetrizer. Equations of motion for the time-dependent orbitals and configuration coefficients are obtained by applying the Dirac-Frenkel variational principle and minimize the norm of the error of the derivative of the wave function with respect to time.

The present implementation for diatomics is based on a previously described [35–37] basis set treatment in prolate spheroidal coordinates using a finite element implementation of the Discrete Variable Representation (DVR) [38–41]. The DVR basis functions are localized on grid points in the prolate spheroidal coordinates $\xi$ and $\eta$, with angular basis functions $e^{im\phi}$ in the azimuthal angle. The (many-electron) ionization continuum is represented rigorously using the method of exterior complex coordinate scaling to apply outgoing wave boundary conditions [42, 43]. Electronic state populations are defined by the overlap between time-independent multiconfiguration self-consistent field (MCSCF) approximations to those states and the time-dependent wave function $|\Psi(t)\rangle$. These wave functions are comprised of nonorthogonal sets of orbitals, and their overlaps are computed using the method described in Appendix A.

The absorption and stimulated emission spectrum is calculated via the response function [44]

$$\tilde{S}^+(\epsilon) = 2\ \mathrm{Im}[D(\epsilon)^* E(\epsilon)] \tag{2}$$

where $E(\epsilon)$ and $D(\epsilon)$ are the Fourier transforms of the electric field and induced dipole moment with respect to energy $\epsilon = \hbar\omega$.

The nuclei are fixed in these calculations, but the pulses are sufficiently short that the results for the transfer of population between electronic states should not be significantly modified by nuclear motion during the pulses.

The bond length is set to $2.175a_0$ (approximately 1.178 Angstrom). We use a DVR grid with 13 points in the prolate spheroidal coordinate $\eta$, in a single finite element, and 15 points per element in $\xi$ with the first element 1 unit long and the rest 4 units long; three such elements are kept on the real axis and the subsequent three are complex scaled at an angle of 0.5 radians. We include factors of $e^{im\phi}$ for $|m| \leq 2$; we check convergence by trying a maximum of $m = 3$. This surprisingly small azimuthal basis is sufficient to reasonably well converge (almost within graphical accuracy) the results presented here, absorption/emission and populations, because outgoing electrons are absorbed via complex scaling when still close to the molecule.

| | 10 orbital | 11 | 12 ($\pi$) | 12 ($\delta$) | Experiment |
|---|---|---|---|---|---|
| B' $^2\Delta$ | 8.63 / *8.40* | 8.73 | 8.49 | 8.60 | 7.48 [45] |
| G $^2\Sigma^-$ | 9.44 | 9.63 | 9.20 | 9.45 | 7.81 [45] |
| I $^2\Sigma^+$ | 9.50 / *7.91* | 9.65 | 9.29 | 9.54 | 7.87 [45] |
| $^2\Delta$ | 400.32 | 400.17 | 400.18 | 400.32 | 399.38 [15] |
| | *406.51* | *406.58* | *406.58* | *406.35* | |
| $^2\Sigma^-$ | 400.77 | 400.72 | 400.54 | 400.80 | 399.71 [15] |
| | *406.04* | *406.31* | *406.76* | *406.19* | |
| $^2\Sigma^+$ | 401.15 | 401.04 | 400.97 | 401.22 | 400.06 [15] |
| | *407.19* | *405.83* | *408.12* | *407.36* | |

TABLE I: Transition energies, in eV, of the relevant electronic states relative to the ground state, calculated with the different orbital bases, with internuclear distance $2.175a_0$, with comparison to standard values from NIST [45] for the valence transitions and those obtained for the core hole transitions from Ref. [15]. Eigenvalues from multiconfiguration self-consistent field calculations are in normal font. Resonant energies, as obtained by propagation with monochromatic fields, as described in subsection IV A, are given in italics.

Calculations were performed using 10-12 orbitals, starting from different multiconfiguration self consistent field (MCSCF) wave functions for the initial state. Once the pulse is applied, symmetry is lost and only the number of orbitals is important. The 10 orbitals are the valence molecular orbitals. For the 11 orbital calculation an additional $\sigma$ orbital is added to the initial state. Two 12 orbital calculations are presented: one with an additional $\pi$ shell, and one with an additional $\delta$ shell in the initial state. Full configuration interaction is used; the resulting Slater determinant bases have 5400, 54450, and 392040 members, respectively. The corresponding spin adapted spaces have dimensions 3300, 29040, and 188760.

## IV. TRANSITION ENERGIES AND AC STARK SHIFTS

We calculate MCSCF wave functions of the ground state for propagation and of excited states for analysis of populations from their projection on the time-dependent wave function. The transition energies from the ground state are listed in normal font in Table I.

Unfortunately, as we found in our prior studies of photoionization [33, 34], transition energies and ionization thresholds apparent in the results of MCTDHF calcula-

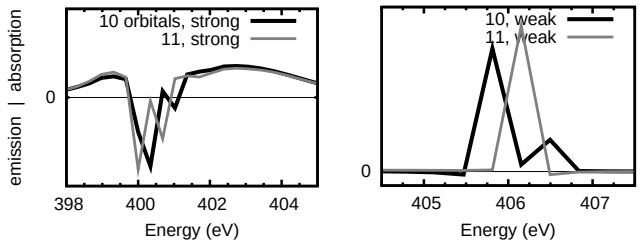


FIG. 3: Absorption (the quantity $\epsilon\ \tilde{S}^{+}(\epsilon)$ calculated from Eq. (2), arbitrary units) calculated with pump laser only, for 10 and 11 orbitals, showing large negative AC stark shift. On the left, the absorption calculated at the intensity used in the stimulated Raman calculation, $5 \times 10^{16}$ W cm$^{-2}$; on the right, that calculated at $5 \times 10^{11}$ W cm$^{-2}$.

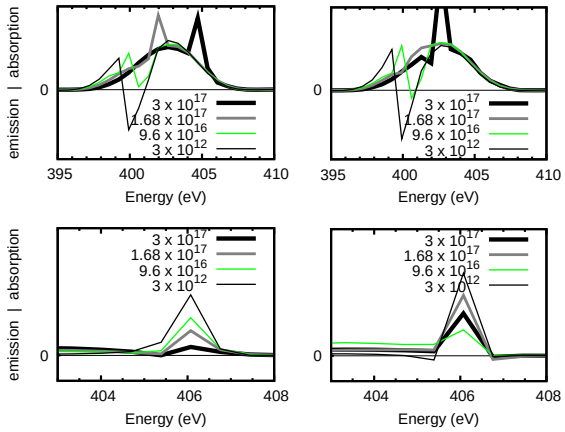


FIG. 4: (Color online) Absorption (the quantity $\epsilon\ \tilde{S}^{+}(\epsilon)$ calculated from Eq. (2), arbitrary units) of the pump laser calculated with both pump and Stokes pulses, varying the strength of the Stokes, for 10 and 11 orbitals. Top: pump laser at $5 \times 10^{16}$W cm$^{-2}$, as in the stimulated Raman calculation. The solid black lines in the top panels correspond to the parameters stimulated Raman calculation with the Stokes at full intensity. Bottom: pump laser at $5 \times 10^{11}$W cm$^{-2}$. Left, 10 orbitals; right, 11.

tions simply do not correspond to those calculated from differences in energies between MCSCF wave functions using the same configuration basis. We have therefore performed a series of calculations to MCTDHF calculations to provide estimates of the transition energies and detunings for an experimental realization of the stimulated Raman population transfer described here.

In Fig. 3 we show the absorption of the pump pulse, for calculations with pump pulse only, both at the intensity of the stimulated Raman calculation, $5 \times 10^{16}$ W cm$^{-2}$, and at $5 \times 10^{11}$ W cm$^{-2}$, at which intensity nonlinear effects are just beginning to be apparent. The results are shown for 10 and 11 orbitals and were calculated by Fourier transforming over 12.5fs. Our analysis of the MCTDHF wave function in Sec. VI below indicates that the $^2\Sigma^+$ state is less populated to the others, and we see no evidence of the $^2\Sigma^+$ state in the calculated absorption signal; the peaks in Fig. 3 are due to the $^2\Sigma^-$ and $^2\Delta$.

In the right panel of Fig. 3, at low intensity, one can see the resonant transitions unaffected by AC stark shifts. The unperturbed transition energies for the $^2\Sigma^-$ and $^2\Delta$ states are approximately 405.75 and 406.5eV with 10 orbitals and both approximately 406.25eV for 11 orbitals.

A very large AC stark shift is apparent in the left panel of Fig. 3, which shows the absorption calculated at high intensity. The AC stark shift with the pump laser alone is approximately -5.5eV for both states for 10 orbitals (shifting them to 400.25 and 401eV), and -6.25 and -5.5eV for the $^2\Sigma^-$ and $^2\Delta$, respectively, for 11 orbitals (shifting them to 400 and 400.75eV).

In Fig. 4, we show the absorption of the pump pulse with the Stokes pulse also included, fixing the strength of the pump, varying the strength of the Stokes, in order to examine the AC stark shift of the pump transition due to the Stokes pulse.

The top panels of Fig. 4 show absorption with the pump laser at $5 \times 10^{16}$W cm$^{-2}$, as in the stimulated Raman calculation; the solid black lines in the top panels correspond to the laser parameters used in the stimulated Raman calculations presented in the sections below. One can see that the combined effect of pump and probe pulses is an AC stark shift that is significantly different for 10 and 11 orbitals.

In the bottom panels of Fig. 4, we show the results fixing the strength of the pump pulse at $5 \times 10^{11}$W cm$^{-2}$. One can see that there is little AC stark shift of the pump transition due to the Stokes pulse alone.

To summarize, the AC stark shift of the pump transition due to the pump pulse alone, or the probe pulse alone, is converged for 10 orbitals; it is the combined effect of the pump and pulse that requires 11 orbitals for convergence of the pump transition AC stark shift. As shown below, even with 11 orbitals the position is only converged to approximately one eV.

### A. Short-time propagation method for transition energies

It is desirable to have a simple method to calculate transition frequencies, without performing a lengthy propagation followed by Fourier transform. We have attempted to devise one, and we have shown the results in italics in Table I.

We performed calculations in which we apply weak monochromatic pulses with instantaneous onset at various frequencies. We calculate populations by taking the overlaps of MCSCF wave functions calculated with the same orbital basis. We then fit the populations as a function of time and laser frequency in order to obtain the transition energies. First order perturbation theory

yields the formula

$$P_n^{(1)}(t) = \left(\frac{\mathscr{E}_0\mu_{n0}}{\hbar}\right)^2 \frac{\sin^2((\omega-\omega_{n0})t/2)}{(\omega-\omega_{n0})^2} \qquad (3)$$

for the population of the $n$th excited state, excited from the ground state and having a transition frequency $\omega_{n0}$ and moment $\mu_{n0}$ relative to it, by a monochromatic field of strength $\mathscr{E}_0$ and frequency $\omega$. To fourth order in time this is

$$P_n^{(1)}(t) = \left(\frac{\mathscr{E}_0\mu_{n0}}{\hbar}\right)^2 \left(\frac{t^2}{4} - \frac{(\omega-\omega_{n0})^2}{48}t^4 + ...\right) \qquad (4)$$

We therefore fit populations $P_n(t)$ at five or six values of $\omega$ to a polynomial fourth order in $t$, and fit the quartic terms obtained to a quadratic polynomial in $\omega$, thereby obtaining $\omega_{n0}$. We verify that the fit is good to visual accuracy and that it does not change if the pulse strength is lowered. The results for the pump transitions are given in italics in Table I.

Unfortunately, due to gauge-dependent oscillations in the populations at the driving frequency $\omega$, and significant dependence upon the state used for projection, the method is evidently accurate only to within about 1eV. The best fits were obtained by using a rotating wave – an unphysical, complex-valued $E(t) = \mathscr{E}_0 e^{-i\omega t}$ – because this reduces oscillations in the populations. Even doing so, the fits we obtained were satisfactory only for a few of the valence transitions.

### B. Performance of the short-time method

If the faster method just described is accurate, it should reproduce the positions of the peaks in Fig. 3. It seems to have done so only approximately. The resonant energies of 406.04 and 406.51eV calculated for the $^2\Sigma^-$ and $^2\Delta$ states are close to the values of 405.75 and 406.5eV estimated (to the nearest quarter eV) from Fig. 3. However the result for $^2\Delta$ with 11 orbitals would imply that a high energy shoulder, at least, should be visible in Fig. 3, but it is not. Clearly, more work is required to define a method for MCTDHF that may easily calculate accurate transition energies for comparison with experiment.

### C. Recommended values for comparison with experiment

We take the 11 orbital result of approximately 406.25eV, obtained by visually examining Fig. 3, to be the transition energies of both the $^2\Sigma^-$ and $^2\Delta$ states. The experimental values of 399.71 and 399.38, respectively [15] are about 6.7eV lower in energy on average. For the valence transition, we note that the resonant energies of 8.40 and 7.91eV calculated for the $^2\Delta$ and $^2\Sigma^+$ are approximately 1eV too high and correct, respectively. We therefore consider our valence transition energies 0.5eV too high on average. Our 402.6 and 393.3eV pulses therefore correspond to an experiment with pulses at 6.7eV and 6.2eV lower energy, respectively, or about 395.9 and 387.1eV. The actual transition energies are about 399.55 up and 391.8eV down on average. This makes the detuning -3.65 and -4.7eV for the pump and Stokes transitions, on average, respectively.

## V. STIMULATED RAMAN SIGNAL

The absorption and emission spectrum is shown in Fig. 5, as calculated via Eq.(2) and by propagating for 50fs in order to converge the features in the Fourier transform. The stimulated Raman signal is indicated by the region in which $\tilde{S}^+(\epsilon)$ is negative.

Fig 5 demonstrates that the 10 orbital result is converged with respect to the azimuthal basis, and velocity gauge precisely agrees with length gauge, as expected. Other than $\approx 1$ eV shifts in peak locations due to large, offsetting AC stark shifts, as discussed in Sec. IV, the results are converged with 11 orbitals. The spectrum of both absorption and emission is described by a high energy peak superimposed upon a lower energy broad absorption band. The broad bands correspond to nonresonant Raman (via the continuum) and follow the Fourier transform of the pulse with the resonant peaks exhibiting Fano profiles on top of that background. In the case of emission the Fano profile of the resonant contribution somewhat obscures the shape of the background contribution, but it can be seen to extend over the range of the Stokes portion of the pulse shown in Fig. 2. The peaks correspond to the resonant Raman transitions we have specified and are resolved to within 1eV.

| State | $M$ | 10 orbital | 11 | 12 ($\pi$) | 12 ($\delta$) | 10 ($m \leq 3$) |
|---|---|---|---|---|---|---|
| X $^2\Pi$ | +1 | 0.0593 | 0.0141 | 0.0007 | 0.0001 | 0.0406 |
| X $^2\Pi$ | -1 | 0.0342 | 0.0200 | 0.0237 | 0.0256 | 0.0351 |
| **G $^2\Sigma^-$** | **0** | **0.0797** | **0.0855** | **0.0916** | **0.0939** | **0.0874** |
| **I $^2\Sigma^+$** | **0** | **0.106** | **0.0908** | **0.0842** | **0.0826** | **0.107** |
| **B' $^2\Delta$** | **+2** | **0.161** | **0.180** | **0.179** | **0.175** | **0.169** |
| **B' $^2\Delta$** | **-2** | **0.0335** | **0.0327** | **0.0365** | **0.0365** | **0.0295** |
| $^2\Sigma^-$ | 0 | 0.0098 | 0.0344 | 0.0406 | 0.0376 | 0.0083 |
| $^2\Sigma^+$ | 0 | 0.0063 | 0.0126 | 0.0174 | 0.0172 | 0.0094 |
| $^2\Delta$ | +2 | 0.0070 | 0.0218 | 0.0314 | 0.0298 | 0.0081 |
| $^2\Delta$ | -2 | 0.0045 | 0.0046 | 0.0039 | 0.0042 | 0.0060 |

TABLE II: Final populations of the electronic states as obtained by projection, for each of the orbital bases. The initial state is X $^2\Pi$, with $M = +1$ projection of angular momentum upon the internuclear axis (first row). States in bold are the final valence states of interest.

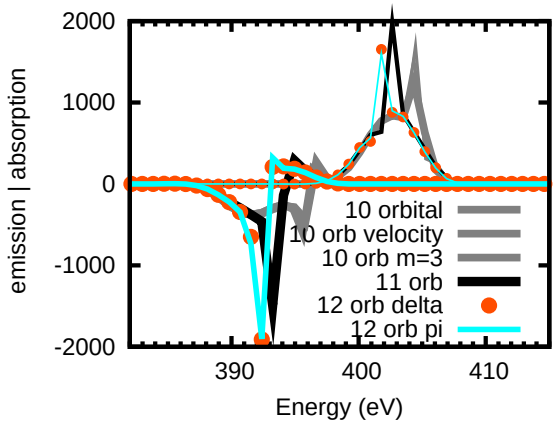


FIG. 5: (Color) Absorption and emission spectra: The unitless function $\epsilon\ \tilde{S}^{+}(\epsilon)$ calculated from Eq. (2) as obtained through Fourier transforms of the dipole moment in the directions parallel (thick lines) and perpendicular (thin lines) to the bond axis, aligned with the Stokes and pump pulses, respectively. Results are shown for four different orbital bases, and for the 10 orbital basis are shown in the length and velocity gauges and also with a larger azimuthal basis (m=3); those lines coincide on the scale of the figure. The integral of the curves is the change in energy (∼50 eV) shown in Fig. 2.

## VI. POPULATION TRANSFER AMONG VALENCE STATES

In Fig. 6 the populations obtained using the four different orbital treatments are shown as a function of time during the pulse. Final valence state populations are listed in Table II in bold, where one can see their convergence to within a root mean square deviation of 1.2 to 5.1% among the 11 and two 12 orbital calculations for the four populations. A population transfer of approximately 40% into the three valence states of interest is achieved and the initial state is almost completely depleted.

At the end of the pulse, the norm-squared of the wave function has decreased from 1 to 0.8 due to the absorption of ionized flux by the exterior complex scaling grid. A rough estimate of the degree of ionization can be made by noting that at 30 fs, the norm-squared is 0.75, and proceeding linearly downward, so that the proportion ionized is probably at least 30%.

The sequential nature of the multiphoton excitations can be seen in the onset of each curve (the point at which it rises above the x axis in Fig. 6). Three points in time can be identified: approximately 0.23fs, 0.45fs, and 0.7fs. At 0.23fs, the core excited state populations in the upper two panels of the figure become significant. At 0.45fs, the two-photon, stimulated Raman process begins to take place: the populations of the valence states become signifcant. Later, at 0.7fs, three photon transitions are apparent. The valence curves appear to have onsets corresponding to two and three photons; the core excited states, the expected one and three.

## VII. CONCLUSIONS

These all-electrons-active calculations have demonstrated that population transfers of order unity can be accomplished with X-ray pulses on a time scale faster than any electronic decoherence that might be caused by nuclear motion. Because this MCTDHF treatment includes a rigorous description of all the ionization continua that constitute principal mechanisms for loss of population to other channels, these calculations provide strong evidence that such experiments will be entirely feasible. The resulting wave packet of the ground state combined with excited $\Sigma$ and $\Delta$ states could be probed in a similar Raman process near the oxygen K-edge and simulated in a further all-electrons active calculation using MCTDHF to provide a diatomic molecule benchmark of the 1D-SXRS experiment recently proposed [2] for polyatomics. The success of these calculations with 15 active electrons demonstrates the potential for the MCTDHF method for electrons to find general utility similar to that of the MCTDH method [46–48] for nuclear dynamics on coupled Born-Oppenheimer potential energy surfaces. The present calculations include 45 linear degrees of freedom, which is comparable in size to the largest MCTDH calculations performed [49–54] without the recursive multilayer treatment [55].

## VIII. ACKNOWLEDGEMENTS

We thank the National Energy Research Supercomputing Center (NERSC) for computational resources. Work performed at Lawrence Berkeley National Laboratory was supported by the US Department of Energy Office of Basic Energy Sciences, Division of Chemical Sciences Contract DE-AC02-05CH11231, and work at the University of California Davis was supported by US Department of Energy grant No. DESC0007182.

### Appendix A: Calculation of electronic populations from MCTDHF wave functions

Electronic state populations are defined by the overlap between a time-independent eigenfunction

$$|\Phi_i\rangle = \sum_{\vec{m}} B_{i\vec{m}} |\vec{m}\rangle \qquad |\vec{m}\rangle = \mathscr{A}\left(|\varphi_{m_1}\rangle \times ... |\varphi_{m_N}\rangle\right) \tag{A1}$$

and the time-dependent wave function $|\Psi(t)\rangle$, comprised of different sets of orbitals. Those overlaps may be written

$$\langle\Phi_i|\Psi(t)\rangle = \sum_{\vec{m}\vec{n}} B^{*}_{i\vec{m}} S_{\vec{m}\vec{n}}(t) A_{\vec{n}}(t) \qquad S_{\vec{m}\vec{n}}(t) = \langle\vec{m}|\vec{n}(t)\rangle \tag{A2}$$

The calculation of the the matrix of overlaps between Slater determinants of nonorthogonal orbitals at many

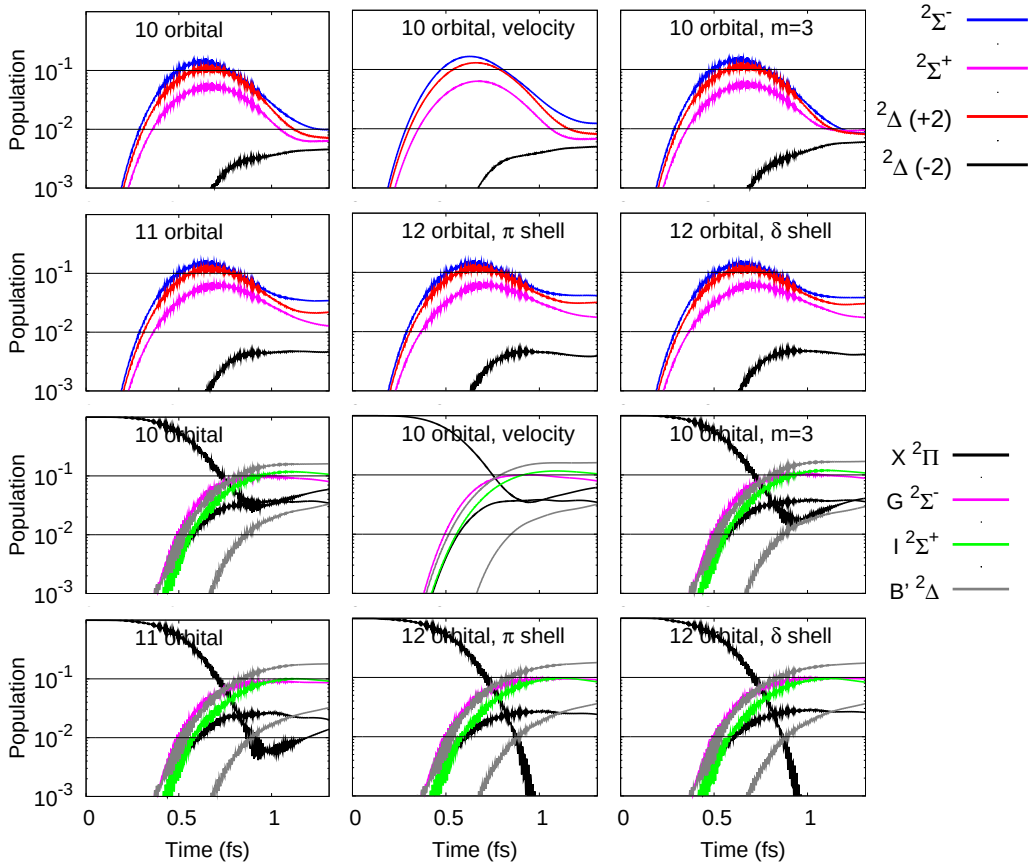


FIG. 6: (Color) Populations during the pulse for calculations with different numbers and types of initial orbitals. Top two rows: populations of core hole states. Bottom two rows: populations of valence states. The molecule begins as $^2\Pi$, $M = +1$, and the populations of the two $M$ components of each of the the degenerate $\Pi$ and $\Delta$ states are plotted separately. Populations are by definition gauge dependent.

values of $t$ presents a computational challenge, but one that can be addressed by an efficient algorithm [33] for full configuration wave functions that does not require dense matrix operations.

The orbital overlap matrix $\mathbf{s}_{ij}(t) = \langle\varphi_i|\phi_j(t)\rangle$ supports an infinite number of matrix logarithms, $\mathbf{ln\ s}$. One of these is chosen and sparse matrix logarithm, $\mathbf{ln\ S}$, of the overlap matrix $\mathbf{S}$ of Eq. (A2) is then constructed by evaluating its matrix elements according to Slater's rules for a one-electron operator with orbital matrix elements $\mathbf{ln\ s}$. Defining

$$\vec{C} = \mathbf{exp}\,(\,\mathbf{ln}\,\boldsymbol{S})\vec{A}\,, \tag{A3}$$

$\langle\Phi_i|\Psi(t)\rangle$ is evaluated as the Hermitian vector dot product of $\vec{B}_i$ and $\vec{C}$. The action of the exponential is performed using a Krylov-space routine [56].

[1] I. V. Schweigert and S. Mukamel, Phys. Rev. Lett. **99**, 163001 (2007).
[2] J. D. Biggs, Y. Zhang, D. Healion, and S. Mukamel, J. Chem. Phys. **136**, 174117 (2012).
[3] S. Mukamel, D. Healion, Y. Zhang, and J. D. Biggs, Ann. Rev. Phys. Chem **64**, 101 (2013).
[4] P. Emma, R. Akre, J. Arthur, R. Bionta, C. Bostedt, J. Bozek, A. Brachmann, P. Bucksbaum, R. Coffee, F.-J. Decker, et al., Nat. Photon. **4**, 641 (2010).
[5] C. Gutt, P. Wochner, B. Fischer, H. Conrad, M. Castro-Colin, S. Lee, F. Lehmkühler, I. Steinke, M. Sprung, W. Roseker, et al., Phys. Rev. Lett. **108**, 024801 (2012).
[6] E. S. Reich, Nature **500**, 13 (2013).
[7] S. Mukamel, Phys. Rev. B **72**, 235110 (2005).
[8] S. Tanaka and S. Mukamel, Phys. Rev. Lett. **89**, 043001 (2002).
[9] N. Rohringer and R. Santra, Phys. Rev. A **77**, 053404 (2008).
[10] L. Young, E. P.-Kanter, B. Krässig, Y. Li, A. M. March, S. T. Pratt, R. Santra, S. H. Southworth, N. Rohringer, L. F. DiMauro, et al., Nature **466**, 56 (2010).
[11] N. Rohringer, D. Ryan, R. A. London, M. Purvis, F. Albert, J. Dunn, J. D. Bozek, C. Bostedt, A. Graf, R. Hill, et al., Nature **481**, 488 (2012).
[12] Y. Morioka, M. Nakamura, E. Ishiguro, and M. Sasanuma, J. Chem. Phys. **61**, 1426 (1974).
[13] N. Kosugi, J. Adachi, E. Shigemasa, and A. Yagishita, J. Chem. Phys. **97**, 8842 (1992).
[14] G. Remmers, M. Domke, A. Puschmann, T. Mandel, G. Kaindl, E. Hudson, and D. A. Shirley, Chem. Phys. Lett. **214**, 241 (1993).
[15] E. Kukk, G. Snell, J. D. Bozek, W.-T. Cheng, and N. Berrah, Phys. Rev. A **63**, 062702 (2001).
[16] R. Fink, J. Chem. Phys. **106**, 4038 (1997).
[17] F. Wang and F. P. Larkins, J. Phys. B **31**, 1649 (1998).
[18] E. Meischer, Can. J. Phys. **54**, 2074 (1976).
[19] M. Sasanuma, Y. Morioka, E. Ishiguro, and M. Nakamura, J. Chem. Phys. **60**, 327 (1974).
[20] R. J. Stubbs, T. A. York, and J. Comer, Chem. Phys. **106**, 161 (1986).
[21] Y. Iida, F. Carnovale, S. Daviel, and C. E. Brion, Chem. Phys. **105**, 211 (1986).
[22] W. F. Chan, G. Cooper, and C. E. Brion, Chem. Phys. **170**, 111 (1993).
[23] P. Erman, A. Karawajczyk, E. Rächlew-Kallne, and C. Strömholm, J. Chem. Phys. **102**, 3064 (1995).
[24] J. Caillat, J. Zanghellini, M. Kitzler, O. Koch, W. Kreuzer, and A. Scrinzi, Phys. Rev. A **71**, 012712 (2005).
[25] O. E. Alon, A. I. Streltsov, and L. S. Cederbaum, J. Chem. Phys. **127**, 154103 (2007).
[26] M. Nest, R. Padmanaban, and P. Saalfrank, J. Chem. Phys. **126**, 214106 (2007).
[27] M. Nest, F. Remacle, and R. D. Levine, New J. Phys. **10**, 025019 (2008).
[28] T. Kato and H. Kono, Chem. Phys. **366**, 46 (2009).
[29] D. Hochstuhl and M. Bonitz, J. Chem. Phys. **134**, 084106 (2011).
[30] R. P. Miranda, A. J. Fisher, L. Stella, and A. P. Horsfield, J. Chem. Phys. **134**, 244101 (2011).
[31] H. Miyagi and L. B. Madsen, Phys. Rev. A **87**, 062511 (2013).
[32] T. Sato and K. L. Ishikawa, Phys. Rev. A **88**, 023402 (2013).
[33] D. J. Haxton, K. V. Lawler, and C. W. McCurdy, Phys. Rev. A **83**, 063416 (2011).
[34] D. J. Haxton, K. V. Lawler, and C. W. McCurdy, Phys. Rev. A **86**, 013406 (2012).
[35] L. Tao, C. W. McCurdy, and T. N. Rescigno, Phys. Rev. A **79**, 012719 (2009).
[36] L. Tao, C. W. McCurdy, and T. N. Rescigno, Phys. Rev. A **80**, 013402 (2009).
[37] L. Tao, C. W. McCurdy, and T. N. Rescigno, Phys. Rev. A **82**, 023423 (2010).
[38] A. S. Dickinson and P. R. Certain, J Chem Phys **49**, 4209 (1968).
[39] G. C. Corey and D. Lemoine, J Chem Phys **97**, 4115 (1992).
[40] J. C. Light, I. P. Hamilton, and J. V. Lill, J Chem Phys **82**, 1400 (1985).
[41] T. N. Rescigno and C. W. McCurdy, Phys. Rev. A **62**, 032706 (2000).
[42] B. Simon, Phys. Lett. **71**, 211 (1979).
[43] C. W. McCurdy, M. Baertschy, and T. N. Rescigno, J. Phys. B **37**, R137 (2004).
[44] D. J. Tannor, *Introduction to Quantum Mechanics: A Time-Dependent Perspective* (University Science Books, New York, 2007).
[45] K. Huber and G. Herzberg, in *NIST Chemistry WebBook, NIST Standard Reference Database Number 69*, edited by P. Linstrom and W. Mallard (National Institute of Standards and Technology, Gaithersburg MD, 20899, 2011).
[46] G. A. Worth, M. H. Beck, A. Jäckle, and H.-D. Meyer, The MCTDH Package, Version 8.2, (2000). See http://www.pci.uni-heidelberg.de/tc/usr/mctdh/.
[47] H.-D. Meyer, U. Manthe, and L. S. Cederbaum, Chem. Phys. Lett. **165**, 73 (1990).
[48] M. H. Beck, A. Jäckle, G. A. Worth, and H.-D. Meyer, Physics Reports **324**, 1 (2000).
[49] M. D. Coutinho-Neto, A. Viel, and U. Manthe, J. Chem. Phys. **121**, 9207 (2004).
[50] O. Vendrell, F. Gatti, D. Lauvergnat, and H.-D. Meyer, J. Chem. Phys. **127**, 184302 (2007).
[51] O. Vendrell, F. Gatti, and H.-D. Meyer, J. Chem. Phys. **127**, 184303 (2007).
[52] O. Vendrell, F. Gatti, and H.-D. Meyer, A. Chemie **46**, 6918 (2007).
[53] T. Hammer and U. Manthe, J. Chem. Phys. **134**, 224305 (2011).
[54] T. Hammer and U. Manthe, J. Chem. Phys. **136**, 054105 (2012).
[55] Q. Meng and H.-D. Meyer, The Journal of Chemical Physics **138**, 014313 (2013), URL `http://scitation.aip.org/content/aip/journal/jcp/138/1/10.1063/1.4772779`.
[56] R. B. Sidje, ACM Trans. Math. Softw. **24**, 130 (1998).